



Freeform 3D deposition of small diameter copper tubes using a powder-binder feedstock

Kedarnath Rane¹ · Matteo Strano²

Received: 27 May 2024 / Accepted: 28 September 2024
© The Author(s) 2024

Abstract

Copper is an interesting material for many applications including thermal management devices, which make often use of copper piping. This study proposes a method for the freeform deposition of a copper-binder feedstock, extruded through an additive manufacturing machine. Several tubes have been printed using a special nozzle and varying process parameters. The dimensional results of the deposited specimens at the green state and the physical properties of the tubes after debinding and sintering have been measured. The results demonstrate that piping in serpentine layout can be deposited by extrusion and sintered, even with sharp bends without significant ovalization of the cross-section.

Keywords 3D deposition · Copper tubes · Powder-binder feedstock · Polymer extrusion

1 Introduction

Copper boasts superior electrical and thermal properties, making it highly suitable for a wide range of applications in electrical and electronic devices, as well as in thermal management systems.

Various attempts have been made to 3D print copper and its alloys using different additive manufacturing techniques, including selective laser melting (SLM) [1], electron beam melting (EBM) [2], and binder jetting [3]. However, the area of 3D printing copper using extrusion-based additive manufacturing has been less explored. Although additive manufacturing by extrusion (EAM) of copper and its alloys is increasingly addressed in scientific literature, a recent review of the research in this field [4] found only about 10 published papers on the topic.

The most common feedstock for extrusion-based additive manufacturing of copper is in the form of filaments, typically made of a mixture of polymeric binder and copper powder [5]. However, a significant drawback of using filaments is the need for binder systems that provide sufficient

mechanical strength and flexibility to allow reliable processing in commercial EAM machines [6]. As a result, the use of copper pastes with pellet extruders has also been proposed [7] and this approach will be utilized in this paper.

Copper and its alloys are valued in additive manufacturing for their effectiveness in thermal management devices [8] (e.g., heat exchanging pipes) and electrical contacts [9]. Previous studies have investigated the mechanical [10], thermal [11] and electrical [12] properties of EAM 3d printed and sintered copper parts. Previous research has also identified the main limitations of copper EAM in these applications such as common defects or problems encountered during 3D printing, debinding, and sintering [13].

One typical problem in all EAM processes of powder-binder feedstock is the large volume fraction of the binder, usually between 45 and 55% [14]. This limitation is inherited from the metal injection moulding (MIM) technology, which can be considered the parent technology [15]. For instance, Moballeghe et al. used three different copper feedstocks with 61.7, 66.2, and 71.2 vol% (94, 95, and 96 wt%) and a thermoplastic binder based on paraffin wax for MIM of copper [16]. They found that the optimum copper feedstock was 66% vol. The high amount of polymeric binder leads to low final density after sintering, although efforts have been made to reduce the binder volume fraction to 33% to achieve fully dense parts [17]. The incomplete infill density during 3D printing also contributes to low final density [18]. A sintered part with reduced density will have decreased thermal and

✉ Matteo Strano
matteo.strano@polimi.it

¹ National Manufacturing Institute Scotland, Glasgow, Scotland, UK

² Dipartimento di Meccanica, Politecnico di Milano, Via La Masa 1, Milan, Italy

electrical conductivity, which are crucial for typical copper applications.

Other consequences of the large volume fraction of the binder are the relatively long processing times for debinding [19] and the significant amount of shrinkage that occurs during sintering [20]. A more severe shrinkage not only reduces the geometrical repeatability of printed parts but may also cause distortions [21, 22] and cracks [23], due to the thermal stresses that develop while debinding and sintering.

Similar to other AM technologies, EAM of copper alloys often requires supports during 3D printing to prevent the collapse of overhanging surfaces [24]. Supports can be printed with the same copper alloys extruded from the main printing nozzle or can be ceramic-based, which dissolve during sintering [25]. However, the presence of supports increases printing times and reduces surface quality [26]. Therefore, most works on 3D printing copper alloys avoid undercuts or overhangs [27]. Yet, typical components for thermal management, such as piping, are inherently hollow and unsupported if printed in non-vertical directions or with complex or bent geometries. Although some examples of 3D printed hollow parts and heat exchange devices exist in the literature, they are usually printed vertically to avoid supports [28]. As an example, Hadian et al. [29] show the extrusion AM of a ceramic nozzle with multiple tubular branches, but all axes of the tubular branches are oriented in the vertical direction and the part is relatively short.

Since tubes are hollow structures, 3d printing the whole circumference poses limitations both in terms of printing time and need for supports. To overcome these limitations, special nozzles (e.g. with a porthole configuration) can be designed for the direct extrusion of hollow cross-sections, reducing or avoiding the need for supports [30] and reducing the extrusion time. However, until now, this approach has only been used for tubes with a straight axis, and the most typical materials used are the ceramic ones [31, 32]. Another interesting example of tube extrusion of ceramic/binder mixtures is reported in [33], where a method is proposed for manufacturing a five-layered micro-tubular structure by a multi-billet co-extrusion process. While ceramic/binder tubes are often extruded, very few examples can be found in the literature on the extrusion of metal/binder mixtures in tubular form. The most typical material used for extruded metal/binder tubes is stainless steel [34, 35], e.g. for the prototypal production of solid oxide fuel cells (SOFCs) [36]. To the authors' knowledge, no paper has been published on the direct tube extrusion of pure copper/binder mixtures, but some work can be found where copper is an alloying element [37].

The above cited papers [29–36] deal with the production by tube extrusion of components with a straight axis. A different approach was proposed in 2004 by Kaya and

Blackburn, who developed a computer-controlled extrusion technique for making ceramic tubes (with a wall thickness of 2 mm and external diameter of 8.0 mm) with tightly controlled bends from ceramic pastes prepared from nano-size boehmite powders [38]. This technique was based on a special extrusion die with changeable internal geometry: small changes in the die alignment causes curvature in the extrudate. The Kaya and Blackburn die was capable of extruding any desired shape, but it was limited to 2D configurations, i.e. it was not embedded in a 3D printing device. The tubes printed in [38] were thick-walled, with a very small wall factor WF (diameter-to-thickness ratio) equal to 4.

The present paper proposes a new method, by testing the freeform deposition of small diameter copper tubes with $WF=4$, using a specially designed porthole nozzle in combination with a 3D printing machine. This system allows for the direct 3D printing of hollow cross-sections without internal supports and enables the production of sharp bends without collapse. Several tube bends were manufactured by varying four process parameters: extrusion velocity V_e , extrusion temperature T_e (i.e. the temperature at the nozzle), layer height h , and transverse feed rate V_t . The sintered tubes were then characterized to evaluate their properties and surface quality.

2 Materials and experimental procedure

2.1 Materials

A commercially available copper metal powder was procured from Sandvik Osprey for the study. It is a copper at 99.4% purity, manufactured by inert gas atomization and usually employed for metal injection moulding of small parts. The metal powder was mixed with a water-soluble binder to form the feedstock. A counter-rotating twin screw Brabender Plasti-Corder mixer with an oil heated chamber at 145 °C for 30 min was used for producing the copper-binder feedstock with a copper powder loading of 63 vol% (92.5% w%) with a final density of the mixture of 6 g/cm³. Figure 1 presents the SEM images of Cu powder and the resulting Cu-binder mixture respectively. The SEM image also illustrates the morphology of the copper particles, which are spherical with a median D_{50} equal to 8.5 μm, a 90th percentile $D_{90}=16$ μm and a 10th percentile $D_{10}=3.5$ μm. The binder is a commercial product (Embemould K83) with a density of 1.45 g/cm³ and it is soluble in water at 20 °C up to 500 g. Its softening point is 115 °C and the melting temperature is 118 °C; its dynamic shear viscosity (DIN 53018) at 150 °C is very low, around 3 Pa s. It cannot be extruded at temperatures above 180 °C because it starts decomposing.

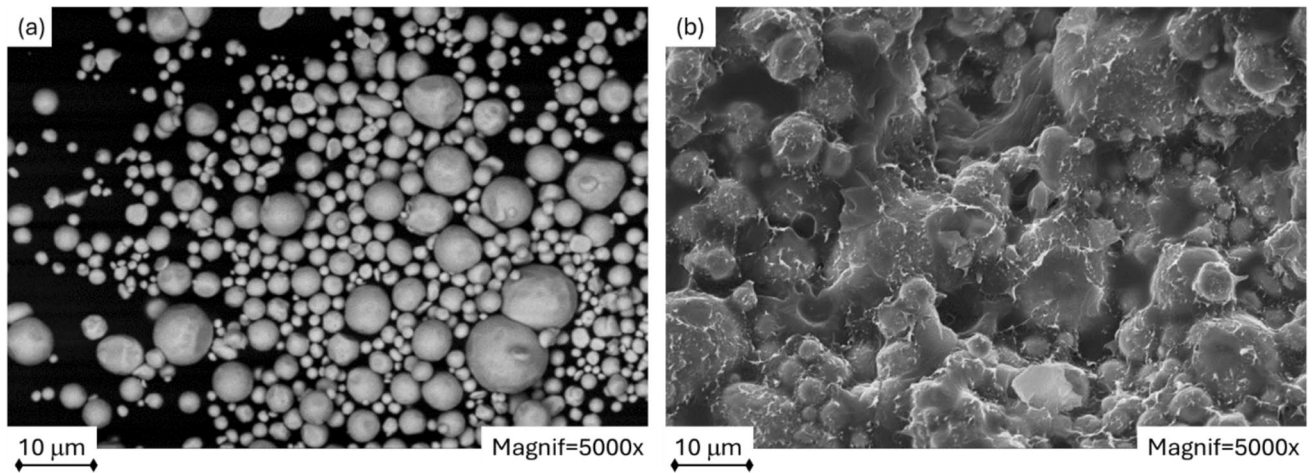


Fig. 1 **a** SEM image of Cu powder; **b** SEM image of Cu-binder feedstock

The viscosity of the obtained copper-binder mixture is obviously much higher, it ranges between 400 and 700 Pa s at 160 °C for shear strain rates between 500 and 5000 s⁻¹. At lower shear rates, below 10 s⁻¹, the shear viscosity of the copper-binder feedstock ranges between 3000 and 5000 Pa s at 160 °C. This viscosity is very well within the range of typical values suggested for EAM applications [39].

To verify the functionality and the versatility of the proposed method, and to verify the openness of the cross-section of the tubes also in the bent region, preliminary tests have been conducted not only with the copper-binder mixture, but also with a pure polymeric feedstock, made of polypropylene (PP) pellets. The extruded PP tubes are partly transparent, allowing for a clear observation of their internal cross-section. The PP pellets are a commercial product (HIPOLEN P FY 6), which is a highly viscous homopolymer designed for extrusion of flat and tubular films, with a melt flow index of MFI = 2.3 g/10 min, according to ASTM D1238 (230 °C; 2.16 kg), which corresponds to a viscosity at low shear rate (below 10 s⁻¹) of 1026 Pa s. The viscosity of the PP at its extrusion temperature is therefore in the same range of the values of the copper-binder feedstock, and it can be considered an acceptable prototype material for the feedstock under investigation.

2.2 3D printing machine and nozzle design

All extrusion and deposition tests have been run with a self-built machine called EFeSTO (Fig. 2a). It is equipped with a parallel kinematics 3-axes “delta” work table placed below a fixed extrusion head [40]. The extrusion head is stationary and composed of a feeder where the pellets of the feedstock are loaded. The pellets fall inside a heated plasticizing cylinder, inclined at 45 °C, where a numerically controlled (NC)

piston squeezes the pellets against a stack of steel balls that provide shear deformation (Fig. 2b).

The pressure of the plasticizing unit injects the melt flow into a vertical injection or extrusion unit, where a NC piston presses the melt flow downward, with a movement synchronized with the work table. The total volume of the injection cylinder is 9000 mm³ and its diameter is 14 mm. Three resistances provide heat to the material: one at the plasticizing unit, one at the injection unit and one at the nozzle. A pneumatic actuated piston closes the channels between the extruder chamber and the nozzle, preventing material loss when the printing job must be stopped or interrupted. From the main injection chamber (A in Fig. 2c), the material flow is divided into two identical sections (B), which further split into two long tubes (C) each. The material flows from these four channels flows into the nozzle region (D). The nozzle is the heart of the newly proposed system, and it is described as follows.

Conventional EAM nozzles are circular in shape and are limited only to extruding and depositing solid beads. To successfully 3D deposit tubes instead of solid beads, a new and special nozzle was designed. The new nozzle has a porthole configuration, it is made of two components: (1) an internal pin equipped with a flange with 6 inlet upstream holes around the central pin; (2) an extrusion die that allows for the creation of a hollow cross-section. A nozzle was designed with internal die diameter of 1.2 mm and a pin diameter of 0.6 mm, producing a wall thickness at the green state of 0.3 mm. Figure 3 shows the drawings of the die, Fig. 4 shows the drawings of the pin and Fig. 5 shows the manufactured nozzle setup.

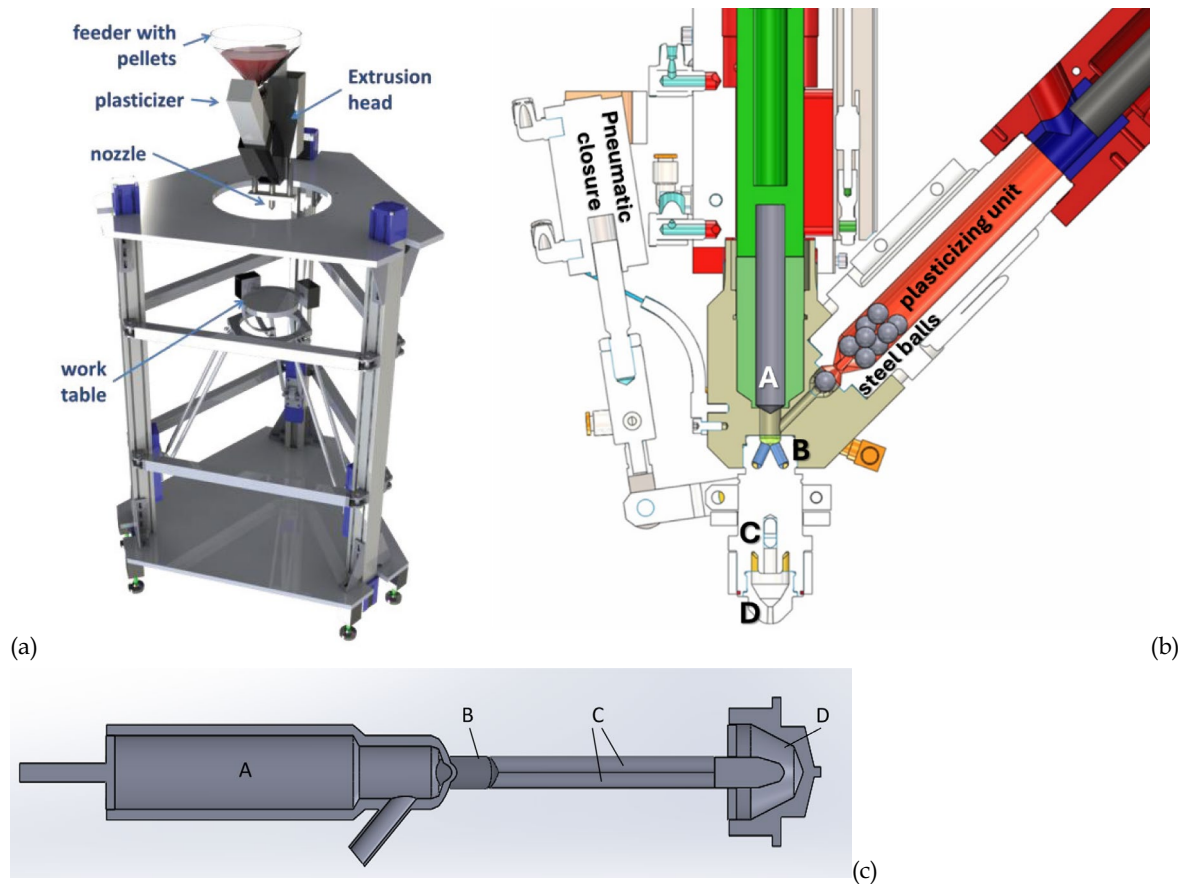
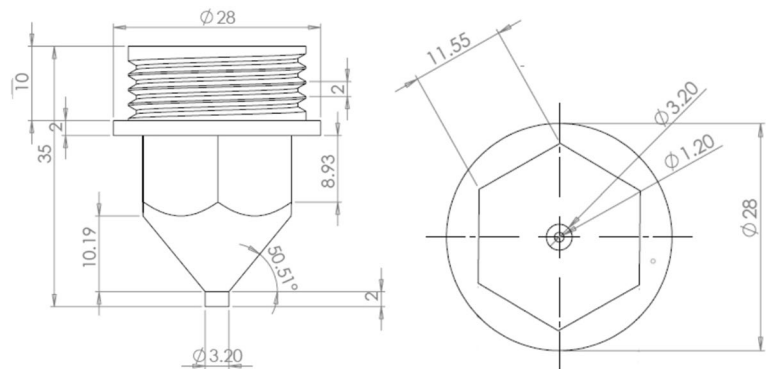


Fig. 2 EFeSTO 3d printing machine (a); cross-section detail of extrusion head (b); cross-section detail of the injection channels (c). A is the main cylinder of the injection unit, B and C are channels downstream the main cylinder, D is the nozzle

Fig. 3 Dimensional drawings of the extrusion die with 1.2 mm diameter



2.3 The extrusion and deposition tests

The typical deposition trajectory used in the tests is a planar serpentine geometry, deployed onto a single plane, with an example of centerline position shown in Fig. 6. The most critical points of this type of trajectory is the bend, which can be characterized by its centerline radius R . The severity of a bend, in traditional tube bending processes of small diameter copper tubes [41], can be assessed by the two

ratios $WF = OD/t_0$ (the wall factor, i.e. the ratio between the tube outer diameter and its thickness) and R/OD (the ratio between the mean centerline radius of the bend and the tube outer diameter). The difficulty of obtaining a bend without collapse of the cross-section (in conventional bending processes) depends on these two factors. The bend becomes more and more difficult as WF increases above 10. In the present case we have a very small wall factor $WF = 4$, i.e. the paper deals with small diameter but thick tubes. The severity

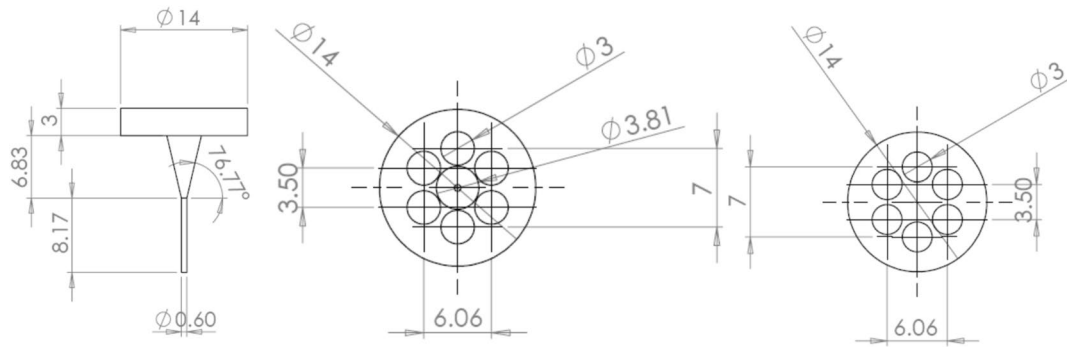


Fig. 4 Dimensional drawings of the pin with 0.6 diameter

Fig. 5 Photos of the manufactured nozzle and pin

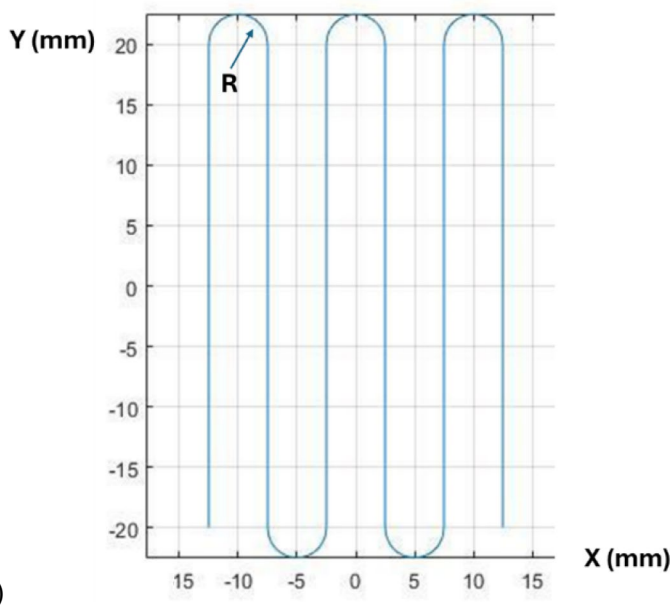


Fig. 6 Trajectory of the deposited tubes with $R/OD=2.1$, X and Y axes in mm (a); example of a green copper serpentine with $R/OD=4.2$, deposited at extrusion velocity $V_e=5$ mm/s, work table

transverse feed rate $V_t=7.5$ mm/s, layer height $h=1.5$ mm and nozzle temperature $T_e=125$ °C (b)

of the bend also increases when the R/OD ratio is small. R/OD ratios below 1.5 are very difficult to obtain in traditional

bending operations, regardless of the wall factor, because the cross-section collapses under the bending stresses. In the

present study, R values greater than or equal to 2.5 mm have been tested (as in Fig. 6a), with a corresponding minimum R/OD factor equal to 2.1, in a safe region. In conclusion, bends have been produced which are not severe, and that can be expected not to be deformed or ovalized under the stresses that develop during the deposition process.

2.4 Debinding and sintering

The part obtained after the deposition process is still “green”, i.e. it requires debinding and sintering, phases that obviously induce shrinkage. The green parts are subjected to a two-stage debinding and a single-stage sintering process after freeform deposition. The obtained green parts were solvent debinded at a uniform temperature of 40 °C in a bath of agitated water for 48 h straight. The parts were then dried completely to ensure thorough removal of moisture from the samples. During the stage of thermal debinding, heating of the parts was carried out in an oven at a heating rate of 20 °C/h up to a temperature of 145 °C with a holding time of 4 h and then at a heating rate of 10 °C/h up to a temperature of 300 °C with a holding time of 2 h, followed by natural cooling in the oven. Finally, sintering of the parts was carried out in an atmosphere of inert gas (argon gas) at a heating rate of 130 °C/h up to a sintering temperature of 1350 °C for 1 h and lastly, the parts were allowed to cool down in the sintering furnace.

2.5 Measurement methods

A scanning electron microscope (Zeiss EVO 50XVP SEM) equipped with a backscattered electron detector (BSE) was utilized to analyze the micrographs of the unsintered and sintered tubes along with the cross-sections of the tubes to check the dimensions and the ovality of the tubes.

The micro-hardness of the sintered copper tubes was also measured using a microhardness tester (FM-810, make:

Future Tech) at 50 gf with a dwell time of 15 s. The tubes were indented at four locations and hardness measurements were taken for each point and then the mean of those measurements was finalized to minimize the probability of errors. Similarly, geometrical deviations were estimated from dimensional measurements of green and sintered tubes.

3 Experimental results and discussion

3.1 Preliminary tests with polypropylene

To verify that the cross-section of the tubes does not collapse nor significantly deforms during the deposition, e.g. because of gravity or because of the bending stresses, preliminary extrusion and deposition tests have been run with polypropylene, changing the extrusion temperature T_e between 180 and 240 °C and the extrusion velocity V_e between 10 and 30 mm/s. Since the PP is transparent, pictures have been taken from portions of the deposited PP tubes and analysed with the image processing software Image-J, after performing some transformation operations. First, the overall geometry has been acquired (example in Fig. 7a) and transformed into a black and white image; then, the outer tube profile has been detected (Fig. 7b) and finally the profile at the internal diameter has been enhanced (Fig. 7c) and detected.

The preliminary results obtained with the PP tubes confirm that the proposed extrusion and deposition strategy is able to deposit tubes with a bent geometry for potential use in thermal management or fluidic applications obtaining an almost circular cross-section not only in the straight portion of the tube but also at the bend. The internal cross-section is completely open and reasonably constant throughout the whole spine of the piping, including the bends.

A very large swelling of the outer tube diameter OD has been observed, with an increase after extrusion of +75% if



Fig. 7 Black and white detail image of a deposited PP tubes with $R/OD=6$ (a); details of outer profile of two tubes with $R/OD=3$ after edge extraction with the software Image J (b); inner profile of a tube with $R/OD=6$ after edge enhancement (c)

extruding at 180 °C. Swelling can be reduced down to +56% if extruding at 240 °C. As shown in Fig. 8, swelling obviously increases with the extrusion velocity, as more material accumulates in the piping. An average increase of the actual wall thickness of +24% has been observed with respect to the nominal wall thickness of the nozzle. In conclusion, the tested polypropylene has shown a strong elastic behaviour.

3.2 Preliminary tests with Cu-binder feedstock

With the encouraging results obtained with the PP tubes (except for the very large swelling), preliminary tests have been conducted for extruding and depositing the Cu-binder feedstock, to explore the technological boundaries of the process. The preliminary tests run with the metal-binder feedstock have allowed to determine:

- the feasible range of the extrusion temperature T_e (between 110 and 150 °C);
- the minimum layer height h (i.e. the distance between the nozzle and the work table) below which the cross-section is deformed (2.5 mm), as shown in Fig. 9a;
- the maximum extrusion velocity V_e (10 mm/s) above which some flow instability phenomena arise, such as the occurrence of the shark skin defect [40] or the vari-

ability of the actual volumetric flow rate vs. the nominal flow rate, as shown in Fig. 9b.

Fixing the feed rate of the work table V_l and the layer height h at constant values, tests have been run with variable extrusion temperature T_e (from 110 to 150 °C) and extrusion velocity V_e (from 2.5 to 15 mm/s), aimed at studying the effect on the tube wall outer diameter and thickness. Swelling of the tube outer diameter OD with the copper feedstock was significantly reduced if compared to the PP, amounting to an average of +7.5%, with a mild influence of the temperature: swelling at 110 °C is 8.2% on average, and it reduces to an average of 6.8% at 150 °C. With respect to the wall thickness, the results are shown in Fig. 10 and they indicate a more prominent role of the temperature, while the extrusion speed is still not statistically significant, given the variability of the results. As the temperature increases, the thickness decreases, because there is a reduced swelling effect.

3.3 Full testing with Cu-binder feedstock: outer diameter and ovality

Exploiting the results of the preliminary tests, a full factorial plan of experiments with four variable factors has been designed, by varying the extrusion temperature T_e , the

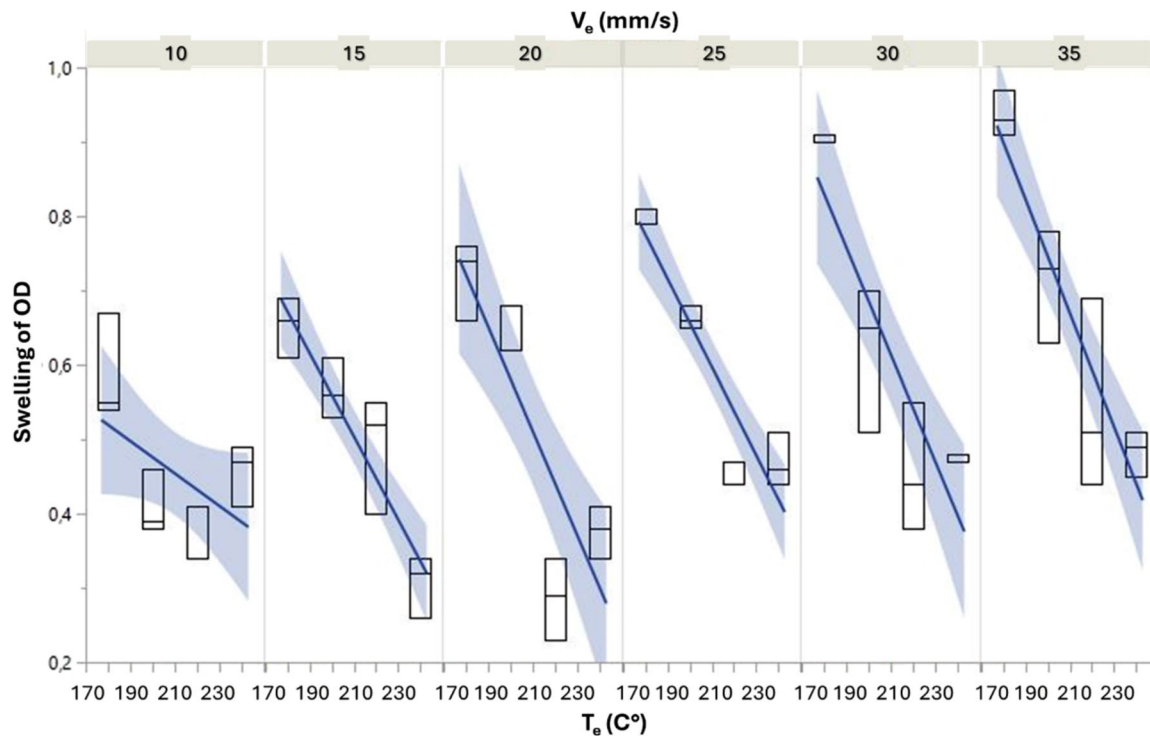


Fig. 8 % Swelling of outer diameter OD of PP tubes as a function of extrusion temperature T_e and velocity V_e ; the plot has been built with the statistical software JMP, it provides the boxplots, a linear regres-

sion trendline for each V_e value and the confidence interval of the prediction yielded by the regression model

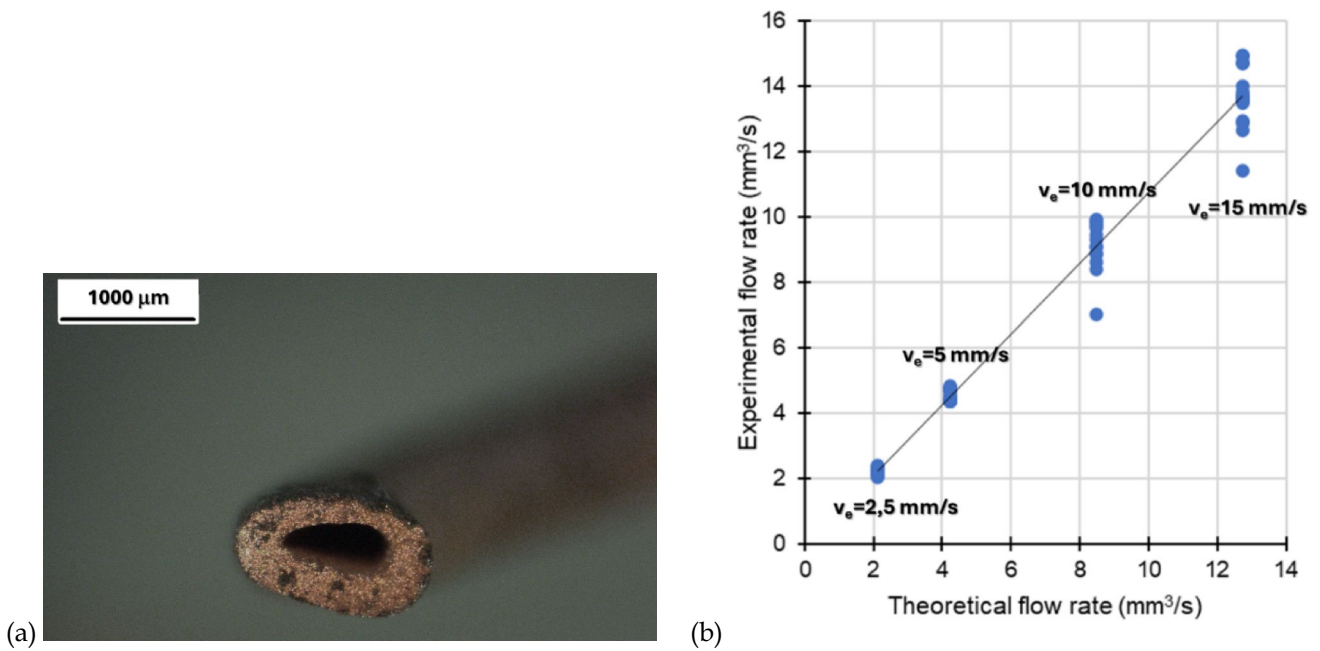


Fig. 9 Flattening of the cross-section of the piping while extruding with $h=1.5$ mm (a); measured vs. predicted volumetric flow rate at different extrusion velocities (b)

Fig. 10 Boxplot and trend-lines showing the influence of temperature on the tube wall thickness at the green state

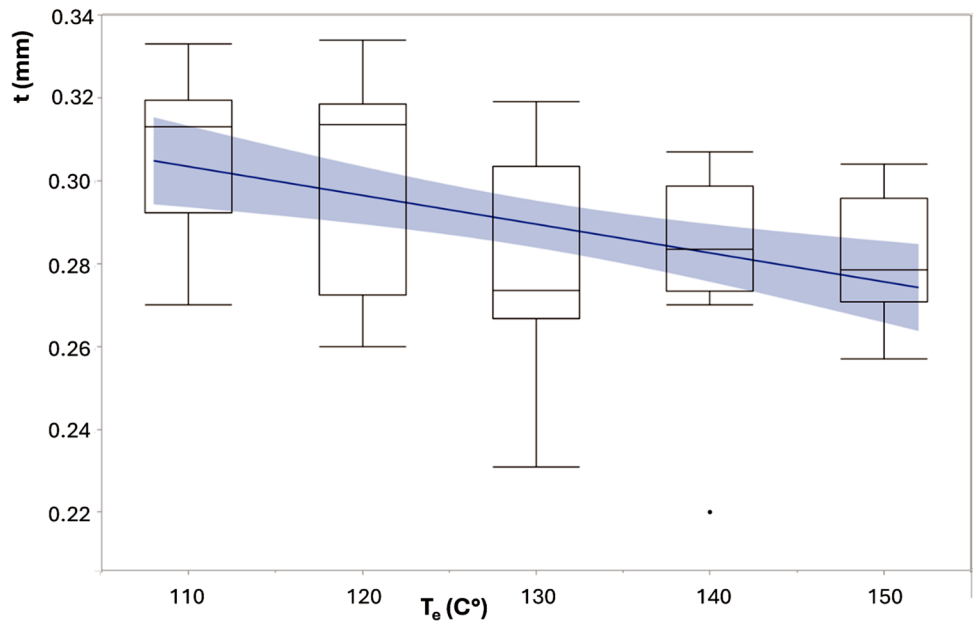


Table 1 Printing parameters for Cu-binder feedstock and their levels for studying the effects on the outer diameter and the ovality of the tubes

Parameters	Levels		
Extrusion temperature, T_e (°C)	110	125	140
Extrusion velocity, V_e (mm/s)	5	7.5	10
V_e/V_t	1	1.25	1.5
Layer height, h (mm)	2.5	3	3.5

extrusion velocity V_e , the work table feed rate V_t and the layer height h . The levels of the process parameters are given in Table 1. A total of 81 experimental conditions has been tested, each condition replicated 2 or 3 times, for a total of 200 tests.

The results indicate that copper tubes can be extruded safely in the whole range of the parameters given in Table 1, in other words, all the 81 tested conditions lead to a feasible process. The dimension of the tubes obtained after the 200

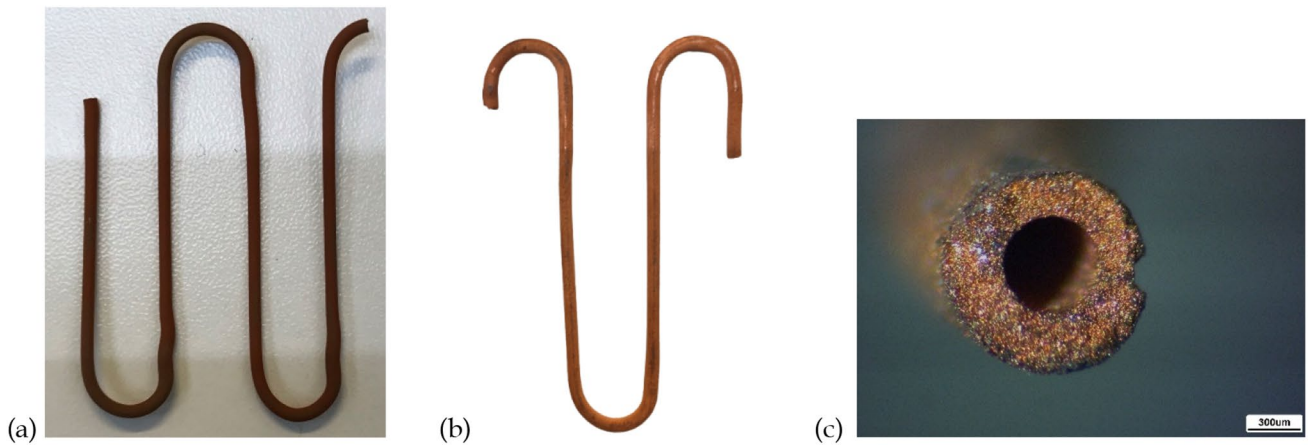


Fig. 11 Green deposited piping (a); portion of a sintered piping (b); micrograph (10×magnification microscope) of the cross-section of a sintered tube (c)

deposition tests have all been measured at the green state, while the sintered dimensions and properties have been measured only for some representative conditions.

Images of both green and sintered copper tubes are shown in Fig. 11. The colour of sintered copper becomes much brighter (Fig. 11b), the cross-section remains open even after sintering (Fig. 11d) in all conditions, despite the obvious considerable liner shrinkage, which has been measured to a grand average of about 13%. Shrinkage reduces both the outer and inner diameter of the tubes; the thickness and the bend radius R are also reduced, therefore, the shrinkage does not significantly change the wall factor WF nor the bend ratio R/OD . The outer diameter OD is not perfectly uniform, and some damages occur occasionally (as also shown in Fig. 11d). An interesting observation is that the sintered dimensions (diameter and thickness) are not very far from the nominal dimensions of the nozzle. As Fig. 11d also

shows, the final wall thickness is very close to the nominal value of $300\ \mu\text{m}$ at the nozzle. The reason is that the green tube undergoes swelling of about +8%, and then it undergoes a shrinkage of about -13% . The combination of the two phenomena leads to a final sintered tube which is only slightly smaller than the designed nozzle cross-section.

In Fig. 12, the surface quality of green and sintered tubes can be observed. In typical 3D printed parts the surface quality is better in the sintered rather than in the green state, because the irregularities between layers and between roads are reduced as an effect of shrinkage [42]. Instead, in the present case the observation of Fig. 12 surprisingly indicates the opposite. The aesthetical quality is much more irregular and non-uniform in the sintered state, because of the presence of oxides and carbonised polymers. The surface mean arithmetic roughness parameter S_a has been measured with a stereomicroscope for samples of both green and sintered

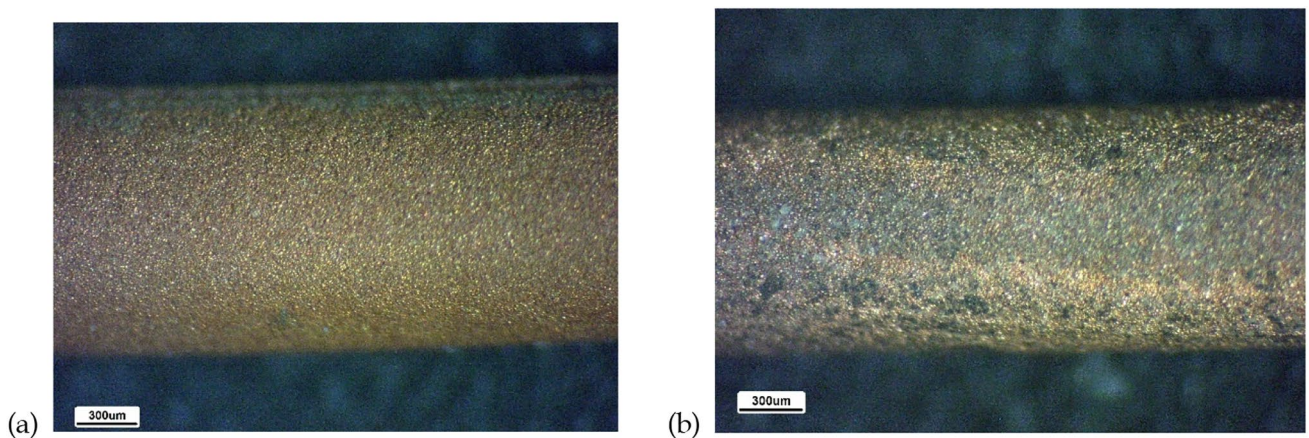


Fig. 12 Micrograph (4.5×magnification microscope) of the surface quality of a green tube in a straight portion (a); micrograph of the outer surface of a sintered tube (b)

tubes, sampling a surface of about 3×1 mm size. These measurements confirmed the differences observed in Fig. 12, in fact S_a is equal to $1.4 \mu\text{m}$ for green tubes and $2.1 \mu\text{m}$ for sintered tubes.

A minimum hardness value of 28 HV, a maximum value of 46 HV and an average of 38 HV were obtained. The results indicate no statistically significant effect of the extrusion temperature and velocity and the other parameters on the hardness of the samples.

The scanning electron microscope (SEM) images reveal the pattern of the particles packing and subsequent densification after the processing steps. Figure 13a shows the cross-section of a green copper tube. It can be seen that the tube has a reasonably good structure with adequate adhesion between the metal

powder particles before debinding and sintering. Figure 13b represents the green part surface morphology of the copper tube viewed at a magnification of $1000\times$ using SEM. A homogenous mixture of the copper powder and the binder can be observed highlighting the spherical morphology of the copper particles. Figure 14 shows instead the tube cross-section after sintering. It can be seen that the tubes have a reasonably little porosity and the tubular shape is well kept after sintering. Thorough removal of the binder from the specimens can be observed. Furthermore, the densification of the particles is clearly visible leaving little to no voids resulting in a high relative density for the tubes.

The dimensional analysis at the green state allows to detect if and how the process parameters influence the outer diameter OD and the percentage ovality $O\%$ (measured as

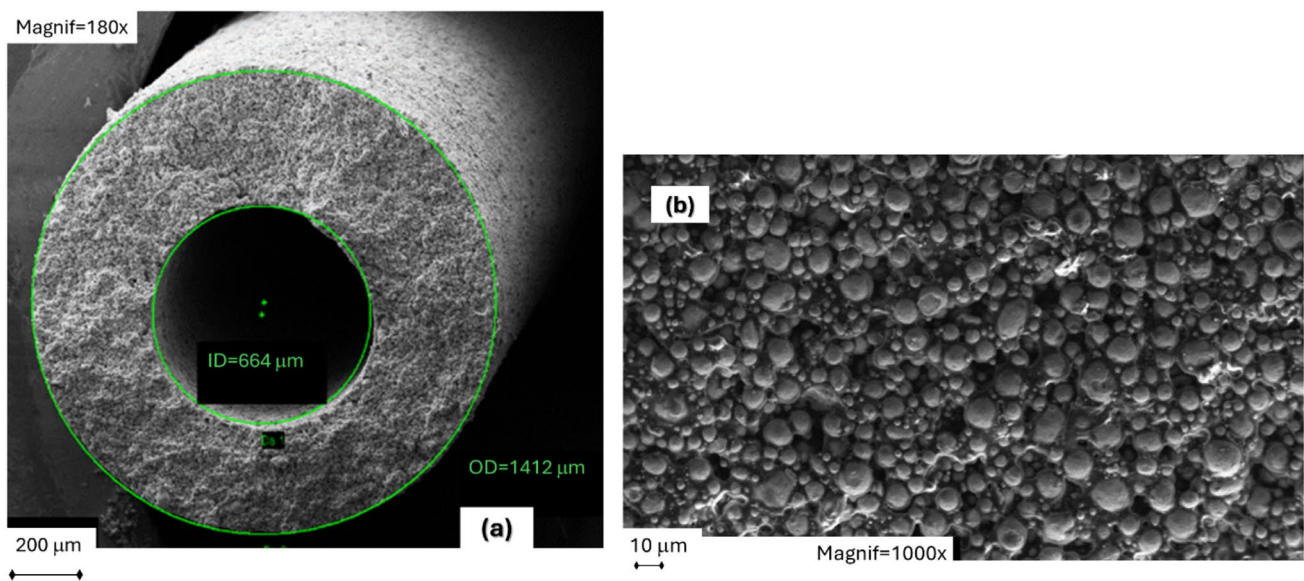


Fig. 13 **a** Cross-section of the green hollow tube and **b** microstructure of the green part surface of the tube

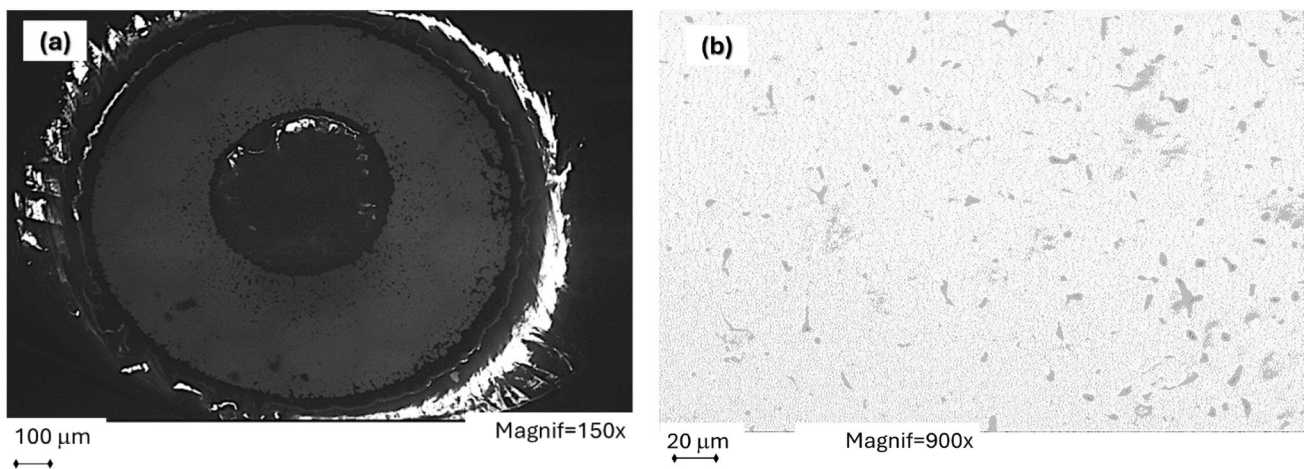
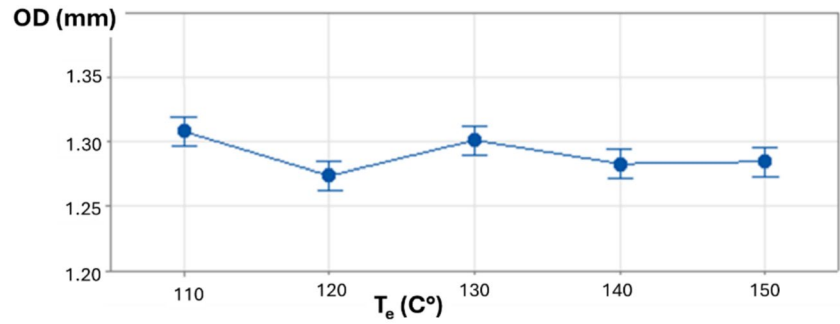


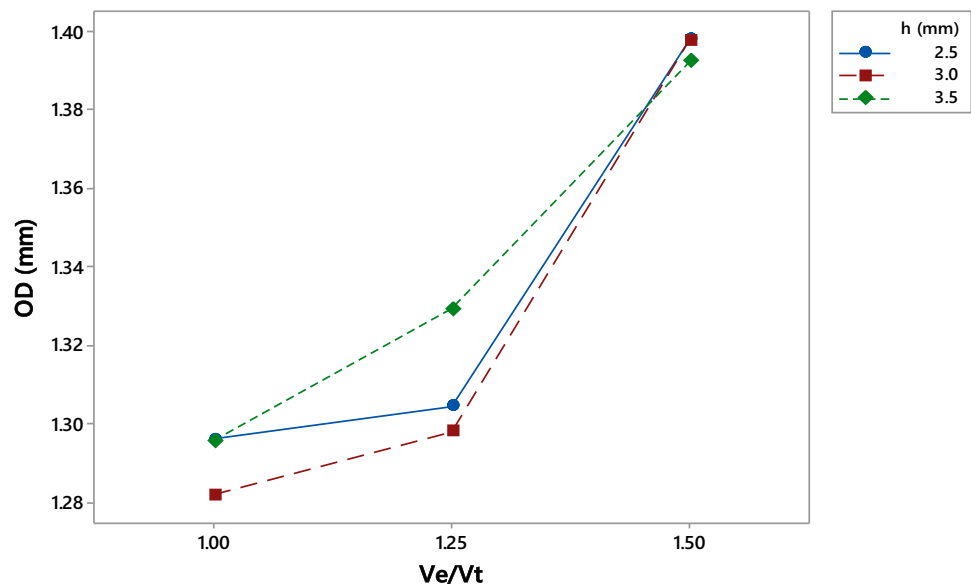
Fig. 14 **a** Cross-section of the sintered hollow tube and **b** microstructure of the sintered part

Fig. 15 Interval plot of OD vs. T_e at the green state (95% confidence interval for the mean, computed using the pooled standard deviation)



the ratio between the minimum and maximum measured diameter and the average diameter). The most significant results are shown in the following figures. Figure 15 shows that, unlike with the PP, the extrusion temperature has practically no influence on the final outer diameter OD and therefore almost no influence on the swelling, with a very mild decreasing trend with increasing temperature. The process has therefore, with respect to temperature, a very large feasibility window. Figure 16 shows, with an interaction plot, how the layer height h and the flow ratio V_e/V_t influence the OD as printed. Unsurprisingly, the diameter swelling increases for increased ratio V_e/V_t , clearly because more volume is extruded while the work table moves, as V_e/V_t increases. When V_e/V_t is equal to 1.5, the diameter grows up to +17% of the nozzle size. The significant effect of V_e/V_t is very useful, because this ratio can be calibrated, in principle, so that the swelling perfectly matches the shrinkage, yielding a final tube dimension that is easier to be predicted. The layer height h has a limited influence on the mean tube diameter, but it is instead (unsurprisingly) important with respect to the ovality of the tube, as shown in Fig. 17. The % ovality deteriorates (increases) when h is small, the best

Fig. 16 Interaction plot of OD vs. h and the ratio V_e/V_t at the green state



value in the investigated range is obtained for $h=3.5$ mm. Ovality also deteriorates when the ratio V_e/V_t increases.

3.4 3D deposition tests

All tests presented in the previous sections have been run by depositing only on a single plane and by using trajectories with relatively large R/OD ratios, greater than 2 (where no significant distortion nor collapse of the cross-section has been observed at the bend). To explore the limits of the proposed process, additional 3D freeform deposition and sintering tests have been run by:

- trying to deposit 3D structures, i.e. superposed layers of serpentines;
- trying to reduce the R/OD ratio of bends down to very small values, as low as 1.25.

Both attempts have been successful, but with some issues discussed as follows.

When depositing full 3D structures, the first deposited layer is supported by the build platform. From the second

Fig. 17 Interaction plot of the tube ovality vs. h and the ratio V_e/V_t at the green state

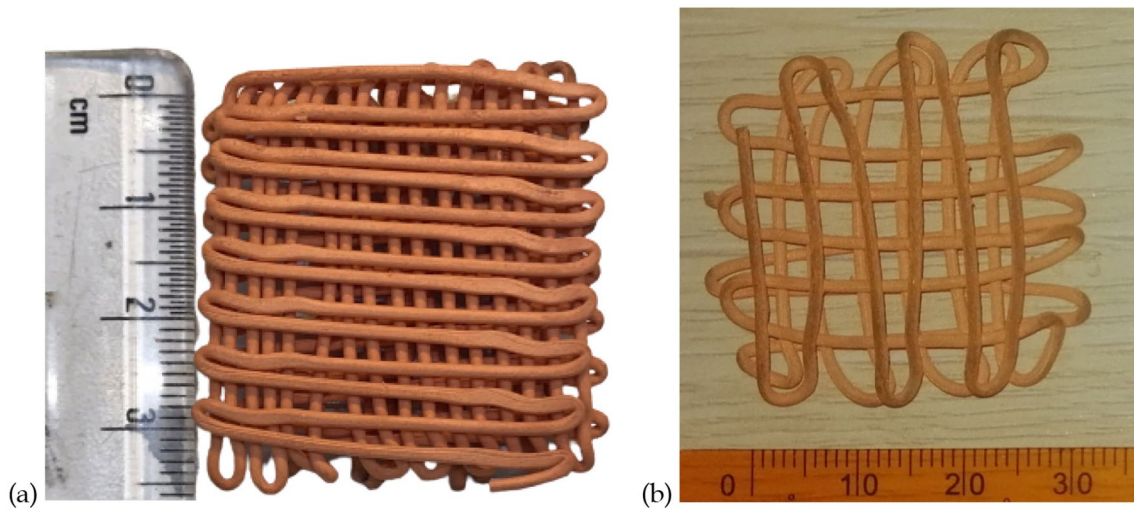
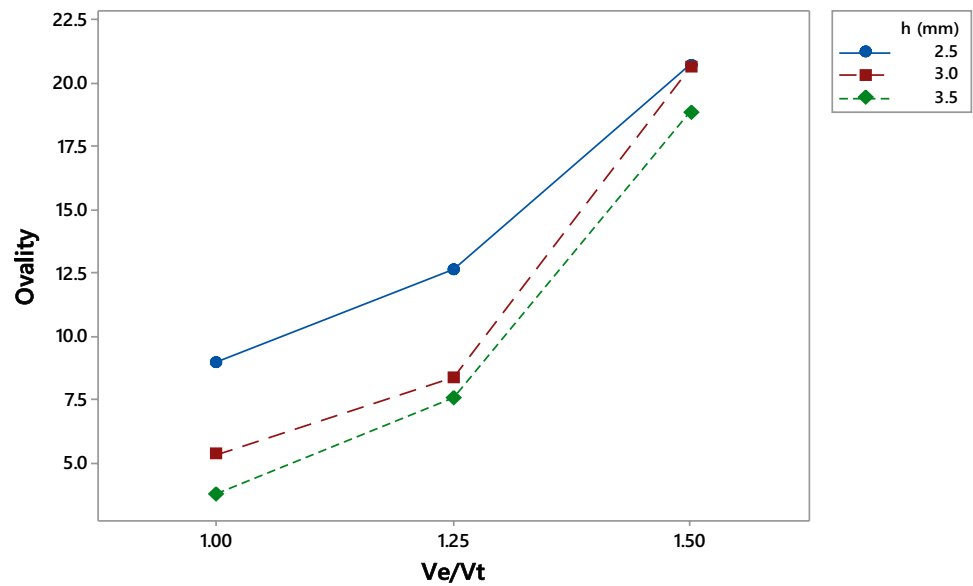


Fig. 18 Green 3D structure printed with $h = 1.5$ mm (a); sintered 3d structures with $h = 2$ mm (b)

layer on, the tube is only partially supported by previous layers, and this deteriorates the geometrical control of the 3D printed structure, yielding to a development of the piping which is not precise (as shown in Fig. 18b). The straightness and the geometrical quality can be improved by reducing the layer height and also by reducing the R/OD ratios, but in this case a strong ovality of the cross-section can be observed (as shown in Fig. 18a). The process can therefore be used for extruding 3D structures, but only if the geometrical precision of the development of the piping is not of crucial importance.

When depositing with a very small R/OD ratio of the bends, the internal cross-section still remains opened and undistorted. However, a variation of the wall thickness distribution occurs, which was not observed in tests with larger R/OD ratio. As very clearly shown in Fig. 19, a cross-section

at the centre of a sharp bend ($R/OD = 1.25$) will have an increased thickness at the intrados of the bend, with a thickness which is nearly double of the thickness measured at the extrados. As in conventional bending processes, the material is compressed at the intrados, and the thickness increases. However, unlike conventional bending processes of solid tubes, no wrinkling has been observed nor collapse of the cross-section. In conclusion, the proposed process appears very effective in producing tubes with very small R/OD ratios, with no defects except for a thickening at the intrados.



Fig. 19 Cross-section of a sintered tube, extruded with $R/OD = 1.25$

4 Conclusions

This study presented a strategy to 3D deposit copper tubes using extrusion-based additive manufacturing with an innovative nozzle design. The deposition strategy proved to be efficient in producing good quality tubes retaining an open and largely undistorted internal channel.

Preliminary tests have been conducted with polypropylene; the tests were successful but the material exhibited a very strong swelling, especially at large extrusion velocity and low extrusion temperature.

The tests conducted with the copper-binder feedstock have shown that the swelling of the extruded cross-section at the green state is more than compensated by the shrinkage that takes place while debinding and sintering. The extrusion temperature has practically no influence on the outer diameter OD. The extruded diameter increases for increased ratio V_e/V_f . The layer height h has a limited influence on the mean tube diameter, but the ovality worsens when h is small, because the material is vertically compressed. Ovality also deteriorates when the ratio V_e/V_f increases. The surface quality of tubes at the green state deteriorates when the tubes are sintered, with the surface roughness parameter S_a that increases by about 30% after sintering.

Tubes can be deposited with 2D planar layouts even with sharp bends with low R/OD ratio, with little ovalization of the cross-section, which remains below 20%. Very sharp bends can be obtained, with $R/OD = 1.25$, at the expense of variation of the wall thickness at the intrados of the tube.

3D layouts can also be deposited, but with loosened control of the obtained geometry.

Acknowledgements The authors express their gratitude to Mr. Ali Kazim Dalkilic, former student of Politecnico di Milano, for his help in the experimental activities.

Author contributions M. Strano: writing—review and editing, resources, investigation, formal analysis, and conceptualization. K. Rane: methodology, investigation, and formal analysis.

Funding Open access funding provided by Politecnico di Milano within the CRUI-CARE Agreement.

Data availability Experimental data are available upon request to the corresponding author.

Declarations

Conflict of interest The authors declare that there are no personal conflicting interests.

Open Access This article is licensed under a Creative Commons Attribution 4.0 International License, which permits use, sharing, adaptation, distribution and reproduction in any medium or format, as long as you give appropriate credit to the original author(s) and the source, provide a link to the Creative Commons licence, and indicate if changes were made. The images or other third party material in this article are included in the article's Creative Commons licence, unless indicated otherwise in a credit line to the material. If material is not included in the article's Creative Commons licence and your intended use is not permitted by statutory regulation or exceeds the permitted use, you will need to obtain permission directly from the copyright holder. To view a copy of this licence, visit <http://creativecommons.org/licenses/by/4.0/>.

References

1. Badrinarayan B, Barlow JW (1991) Selective laser sintering of a Copper-PMMA system. In: Proceedings of the solid freeform fabrication symposium, Austin, TX, USA, pp 245–250
2. Frigola P, Harrysson O, Horn TJ, West H, Aman R, Rigsbee JM, Ramirez DA, Murr L, Medina F, Wicker RB, Rodriguez E (2014) Fabricating copper components with electron beam melting. *Adv Mater Process* 172:20–24
3. Bai Y, Williams Christopher B (2015) An exploration of binder jetting of copper. *Rapid Prototyp J* 21:177–185. <https://doi.org/10.1108/RPJ-12-2014-0180>
4. Sakib-Uz-Zaman C, Khondoker MAH (2023) A review on extrusion additive manufacturing of pure copper. *Metals (Basel)* 13:859. <https://doi.org/10.3390/met13050859>
5. Gonzalez-Gutierrez J, Cano S, Ecker JV, Kitzmantel M, Arbeiter F, Kukla C, Holzer C (2021) Bending properties of lightweight copper specimens with different infill patterns produced by material extrusion additive manufacturing, solvent debinding and sintering. *Appl Sci* 11:7262. <https://doi.org/10.3390/app11167262>
6. Sadaf M, Cano S, Gonzalez-Gutierrez J, Bragaglia M, Schuschnigg S, Kukla C, Holzer C, Vály L, Kitzmantel M, Nanni F (2022) Influence of binder composition and material extrusion (MEX) parameters on the 3D printing of highly filled copper feedstocks. *Polymers (Basel)* 14:4962. <https://doi.org/10.3390/polym14224962>
7. Singh G, Missiaen J-M, Bouvard D, Chaix J-M (2021) Copper extrusion 3D printing using metal injection moulding feedstock: analysis of process parameters for green density and surface roughness optimization. *Addit Manuf* 38:101778. <https://doi.org/10.1016/j.addma.2020.101778>

8. Singer F, Deisenroth DC, Hymas DM, Ohadi MM (2017) Additively manufactured copper components and composite structures for thermal management applications. In: 2017 16th IEEE intersociety conference on thermal and thermomechanical phenomena in electronic systems (ITherm), IEEE, pp 174–183. <https://doi.org/10.1109/ITHERM.2017.7992469>
9. Cañadilla A, Rodríguez G, Romero A, Caminero MA, Dura OJ (2024) Sustainable production of copper components using concentrated solar energy in material extrusion additive manufacturing (MEX-CSE). *Sustain Mater Technol* 39:e00799. <https://doi.org/10.1016/j.susmat.2023.e00799>
10. Cañadilla A, Romero A, Rodríguez GP, Caminero MÁ, Dura ÓJ (2022) Mechanical electrical, and thermal characterization of pure copper parts manufactured via material extrusion additive manufacturing. *Materials* 15:4644. <https://doi.org/10.3390/ma15134644>
11. Dehdari Ebrahimi N, Ju YS (2018) Thermal conductivity of sintered copper samples prepared using 3D printing-compatible polymer composite filaments. *Addit Manuf* 24:479–485. <https://doi.org/10.1016/j.addma.2018.10.025>
12. Hwang JY, Jung HY (2024) Electrical conductivity upon sintering of pure Cu produced by material extrusion additive manufacturing: effects of pore, grain size, and impurity. *J Manuf Process* 118:63–75. <https://doi.org/10.1016/j.jmapro.2024.03.049>
13. Meng F, Beretta M, Pellegrini A, Selema A, Sergeant P, Vleugels J, Galantucci LM, Ferraris E (2024) Impact of strand deposition and infill strategies on the properties of monolithic copper via material extrusion additive manufacturing. *Addit Manuf* 89:104277. <https://doi.org/10.1016/j.addma.2024.104277>
14. Ren L, Zhou X, Song Z, Zhao C, Liu Q, Xue J, Li X (2017) Process parameter optimization of extrusion-based 3D metal printing utilizing PW-LDPE-SA binder system. *Materials* 10:305. <https://doi.org/10.3390/ma10030305>
15. Ul Mohsin I, Lager D, Gierl C, Hohenauer W, Danninger H (2011) Simulation and optimisation for thermal debinding of copper MIM parts using thermokinetic analysis. *Powder Metall* 54:30–35. <https://doi.org/10.1179/003258910X12740974839620>
16. Moballeghe L, Morshedjan J, Esfandeh M (2005) Copper injection molding using a thermoplastic binder based on paraffin wax. *Mater Lett* 59:2832–2837. <https://doi.org/10.1016/j.matlet.2005.04.027>
17. Kolli S, Beretta M, Selema A, Sergeant P, Kestens LAI, Rombouts M, Vleugels J (2023) Process optimization and characterization of dense pure copper parts produced by paste-based 3D micro-extrusion. *Addit Manuf* 73:103670. <https://doi.org/10.1016/j.addma.2023.103670>
18. Hong S, Sanchez C, Du H, Kim N (2015) Fabrication of 3D printed metal structures by use of high-viscosity Cu paste and a screw extruder. *J Electron Mater* 44:836–841. <https://doi.org/10.1007/s11664-014-3601-8>
19. Yan X, Wang C, Xiong W, Hou T, Hao L, Tang D (2018) Thermal debinding mass transfer mechanism and dynamics of copper green parts fabricated by an innovative 3D printing method. *RSC Adv* 8:10355–10360. <https://doi.org/10.1039/C7RA13149F>
20. Wei X, Behm I, Winkler T, Bähr R (2024) Optimization of extrusion-based additive manufacturing of bronze metal parts using a CuSn10/polylactic acid composite. *J Market Res* 30:3602–3610. <https://doi.org/10.1016/j.jmrt.2024.04.111>
21. Kılınç AÇ, Goktas AA, Keskin ÖY, Köktaş S (2021) Extrusion-based 3D printing of CuSn10 bronze parts: production and characterization. *Metals (Basel)* 11:1774. <https://doi.org/10.3390/met11111774>
22. Wei X, Li X, Bähr R (2024) Optimizing metal part distortion in the material extrusion-thermal debinding-sintering process: an experimental and numerical study. *Heliyon* 10:e28899. <https://doi.org/10.1016/j.heliyon.2024.e28899>
23. Liu S, Li Y, Xing S, Liu L, Zou G, Zhang P (2019) Structure inheritance in nanoparticle ink direct-writing processes and crack-free nano-copper interconnects printed by a single-run approach. *Materials* 12:1559. <https://doi.org/10.3390/ma12091559>
24. Jiang J, Xu X, Stringer J (2018) Support structures for additive manufacturing: a review. *J Manuf Mater Process* 2:64. <https://doi.org/10.3390/jmmp2040064>
25. Rane K, Strano M (2019) A comprehensive review of extrusion-based additive manufacturing processes for rapid production of metallic and ceramic parts. *Adv Manuf* 7:155–173. <https://doi.org/10.1007/s40436-019-00253-6>
26. Singh G, Missiaen J-M, Bouvard D, Chaix J-M (2021) Copper additive manufacturing using MIM feedstock: adjustment of printing, debinding, and sintering parameters for processing dense and defectless parts. *Int J Adv Manuf Technol* 115:449–462. <https://doi.org/10.1007/s00170-021-07188-y>
27. Jin K, Li G, Wei B, Chen R, Chen P, Cheng J (2024) Preparation of bronze (CuSn10) parts by material extrusion process using paraffin-based binder. *J Mater Eng Perform*. <https://doi.org/10.1007/s11665-024-09455-x>
28. Rane K, Cataldo S, Parenti P, Sbaglia L, Mussi V, Annoni M, Giberti H, Strano M (2018) Rapid production of hollow SS316 profiles by extrusion based additive manufacturing. In: AIP conf proc, p 140014. <https://doi.org/10.1063/1.5035006>
29. Hadian A, Morath B, Biedermann M, Meboldt M, Clemens F (2023) Selected design rules for material extrusion-based additive manufacturing of alumina based nozzles and heat exchangers considering limitations in printing, debinding, and sintering. *Addit Manuf* 75:103719. <https://doi.org/10.1016/j.addma.2023.103719>
30. Chen Z, Ikeda K, Murakami T, Takeda T, Xie J-X (2003) Fabrication of composite pipes by multi-billet extrusion technique. *J Mater Process Technol* 137:10–16. [https://doi.org/10.1016/S0924-0136\(02\)01052-X](https://doi.org/10.1016/S0924-0136(02)01052-X)
31. Liang D, Huang J, Zhang H, Fu H, Zhang Y, Chen H (2021) Influencing factors on the performance of tubular ceramic membrane supports prepared by extrusion. *Ceram Int* 47:10464–10477. <https://doi.org/10.1016/j.ceramint.2020.12.235>
32. Azzolini A, Downs J, Sglavo VM (2015) Fabrication and co-sintering of thin tubular IT-SOFC with Cu₂O-GDC cermet supporting anode and Li₂O-doped GDC electrolyte. *J Eur Ceram Soc* 35:2119–2127. <https://doi.org/10.1016/j.jeurceramsoc.2015.01.023>
33. Powell J, Blackburn S (2010) Co-extrusion of multilayered ceramic micro-tubes for use as solid oxide fuel cells. *J Eur Ceram Soc* 30:2859–2870. <https://doi.org/10.1016/j.jeurceramsoc.2010.02.010>
34. Li S-B, Xie J-X (2007) Fabrication of thin-walled 316L stainless steel seamless pipes by extrusion technology. *J Mater Process Technol* 183:57–61. <https://doi.org/10.1016/j.jmatprotec.2006.09.024>
35. Kuriakose S, Cataldo S, Parenti P, Annoni M (2020) Debinding and presintering of high aspect ratio micro-lumen tubes produced by extrusion of 17–4PH feedstock. *J Micro Nanomanuf.* <https://doi.org/10.1115/1.4046562>
36. Sotomayor ME, Levenfeld B, Várez A (2011) Powder extrusion moulding of 430L stainless steel thin tubes for porous metal supported SOFCs. *Powder Metall* 54:103–107. <https://doi.org/10.1179/003258909X12502679013693>
37. Han S, Cui L, Li D (2018) W–Cu tube processing and structure property by powder extrusion molding. In: High performance structural materials. Springer Singapore, Singapore, pp 1003–1010. https://doi.org/10.1007/978-981-13-0104-9_105
38. Kaya C, Blackburn S (2004) Extrusion of ceramic tubes with complex structures of non-uniform curvatures made from nano-powders. *J Eur Ceram Soc* 24:3663–3670. <https://doi.org/10.1016/j.jeurceramsoc.2003.12.012>
39. Khaliq MH, Gomes R, Fernandes C, Nóbrega J, Carneiro OS, Ferrás LL (2017) On the use of high viscosity polymers in the fused filament fabrication process. *Rapid Prototyp J* 23:727–735. <https://doi.org/10.1108/RPJ-02-2016-0027>

40. Rane K, Barriere T, Strano M (2020) Role of elongational viscosity of feedstock in extrusion-based additive manufacturing of powder-binder mixtures. *Int J Adv Manuf Technol* 107:4389–4402. <https://doi.org/10.1007/s00170-020-05323-9>
41. Mentella A, Strano M (2012) Rotary draw bending of small diameter copper tubes: predicting the quality of the cross-section. *Proc Inst Mech Eng B J Eng Manuf* 226:267–278. <https://doi.org/10.1177/0954405411416306>
42. Rane K, Petrò S, Strano M (2020) Evolution of porosity and geometrical quality through the ceramic extrusion additive manufacturing process stages. *Addit Manuf* 32:101038. <https://doi.org/10.1016/j.addma.2020.101038>

Publisher's Note Springer Nature remains neutral with regard to jurisdictional claims in published maps and institutional affiliations.